

Temperature Structure of the Pipe Nebula Studied by the Intensity Anomaly of the OH 18 cm Transition

YUJI EBISAWA,¹ NAMI SAKAI,² KARL M. MENTEN,³ YOKO OYA,¹ AND SATOSHI YAMAMOTO¹

¹*Department of Physics, The University of Tokyo, Hongo, Bunkyo-ku, Tokyo 113-0033, Japan*

²*RIKEN, 2-1 Hirosawa, Wako, Saitama 351-0198, Japan*

³*Max-Planck-Institut für Radioastronomie, Auf dem Hügel 69, D-53121 Bonn, Germany*

ABSTRACT

We present observations of the four hyperfine structure components of the OH 18 cm transition (1612, 1665, 1667 and 1720 MHz) toward a filamentary dark cloud, the Pipe nebula, with the Green Bank Telescope. A statistical equilibrium analysis is applied to the spectra, and the kinetic temperature of a diffuse molecular gas surrounding dense cores is determined accurately; the derived temperature ranges from 40 K to 75 K. From this result, we assess the heating effect on the filamentary structure of the nebula’s “stem” region due to UV photons from a nearby star θ -Ophiuchi and a possible filament-filament collision in the interface of the “stem” and “bowl” regions. In the stem region, the gas kinetic temperature is found to be almost independent of the apparent distance from θ -Ophiuchi: the UV-heating effect by the star is not visible. On the other hand, the gas kinetic temperature is raised, as high as ~ 75 K, at the interface of the two filamentary structures. This result provides us with an additional support to the filament-filament collision scenario in the Pipe nebula.

Keywords: ISM: molecules - ISM: individual objects (Pipe nebula)

1. INTRODUCTION

The 18 cm transition of the hydroxyl radical (OH) has extensively been observed toward molecular clouds, late-type stars and external galaxies (e.g. Harju et al. 2000; Caswell 2004; Hoffman et al. 2005; Wolak et al. 2012; Darling & Giovanelli 2002; Ebisawa et al. 2015, 2019; Li et al. 2018; Xu et al. 2016). It is the Λ -type doubling transition in the ground rotational state, and consists of the four hyperfine structure (hfs) lines at 1612, 1665, 1667, and 1720 MHz. It is well known that the observed intensity ratio of the four hfs lines is often different from the ratio expected in the local thermodynamic equilibrium (LTE) condition; $I_{1612} : I_{1665} : I_{1667} : I_{1720} = 1 : 5 : 9 : 1$ (e.g. Harju et al. 2000; Ebisawa et al. 2015). Such intensity anomalies can be caused by collisional and/or radiative processes among the rotational states (Elitzur et al. 1976; van Langevelde et al. 1995; Ebisawa et al. 2019). Ebisawa et al. (2015), on the basis of their statistical equilibrium calculations, reported that the intensity ratio is sensitive to the gas kinetic temperature. They demonstrated that the gas kinetic temperature of warm ($T_k > 30$ K) molecular clouds can be determined accurately from the observed intensities. Furthermore, the critical density of the OH 18 cm transition is so low ($< 10^2 \text{ cm}^{-3}$) that a diffuse molecular gas surrounding dense cores, which is generally difficult to trace by rotational transitions of CO (i.e. so-called CO-dark gas), could be observed by the OH 18 cm transition (Ebisawa et al. 2015; Xu et al. 2016; Tang et al. 2017). In this paper, this method for temperature determination is applied to a nearby molecular cloud, the Pipe nebula.

The Pipe nebula is a filamentary ($\sim 3 \text{ pc} \times 18 \text{ pc}$) massive ($\sim 10^4 M_\odot$) molecular cloud complex (Frau et al. 2015), that was first identified in the lines of CO and its isotopologues by Onishi et al. (1999). Figure 1 shows the 2MASS visual extinction (A_K) map observed for the whole part of the Pipe nebula (Lombardi et al. 2006). As shown in Figure 1, the Pipe nebula roughly consists of three regions; B59 at the western end, the stem region having a characteristic filamentary structure, and the bowl region exhibiting an extended structure in the eastern part. Since the Pipe nebula is a nearby ($\sim 145 \text{ pc}$) object (Alves & Franco 2007) with little star formation activity except for the B59 region (Onishi et al. 1999), it has been a good target to study molecular-cloud formation (Lada et al. 2008; Román-Zúñiga et al. 2010). Its magnetic-field structure has been investigated by polarimetry

(Alves et al. 2008, 2014; Franco et al. 2010). A bright B2 IV star, θ Ophiuchi (HD 157056), is located at about 3 pc away from the Pipe nebula (Figure 1), and feedback with this star has been invoked for shaping the structure and the formation process of the nebula (Onishi et al. 1999; Gritschneider & Lin 2012).

The velocity structure of the Pipe nebula was studied in the ^{12}CO and its isotopologue lines. Figure 2 shows the integrated intensity maps of the ^{13}CO ($J = 1 - 0$) (cyan contours) and ^{12}CO ($J = 1 - 0$) (red contours) lines by Onishi et al. (1999) overlaid on the visual extinction (A_K) map of Figure 1. The ^{12}CO map is prepared by integrating over the velocity range from 6 to 10 km s $^{-1}$ (Onishi et al. 1999). As shown in Figure 2, the ^{13}CO line traces a filamentary structure elongated along the west to east direction, which is seen in the visual extinction map. We hereafter call this structure the W-E filament. On the other hand, the ^{12}CO map exhibits another filamentary structure extending along the south to north direction (S-N filament) which is perpendicular to the W-E filament. According to Frau et al. (2015), the W-E filament has a blue-shifted velocity (V_{LSR} of 2–4 km s $^{-1}$), whereas the S-N filament has a red-shifted velocity (V_{LSR} of 6–7 km s $^{-1}$). These two filamentary structures overlap on the bowl region. On the basis of their combined analyses of the optical polarimetry, the visual extinction, and ^{13}CO data, Frau et al. (2015) suggested that these two structures are colliding with each other in the overlapping region. They found that the gas in the bowl region tends to show a higher density and a broader linewidth, as well as a stronger polarization degree and a smaller dispersion of polarization angle in the optical observations. These results are discussed in terms of compressive motion caused by a filament-filament collision.

In this study, we investigate the nature of the Pipe nebula by focusing on the following two effects: (1) UV heating from θ -Oph, and (2) collisions between the W-E and S-N filaments. For this purpose, we explore a temperature structure of the Pipe nebula by observing the OH 18 cm transition. If the Pipe nebula were affected by UV heating from θ -Oph, the gas kinetic temperature would increase with a decreasing distance from θ -Oph. In addition, the temperature would be raised at the interface of the two filaments, if a filament-filament collision occurred. We examine these two effects on the basis of our statistical equilibrium calculations for the OH 18 cm transition.

2. OBSERVATION

We observed the four hfs components of the OH 18 cm transition toward the Pipe nebula with the Robert C. Byrd Green Bank Telescope (GBT) in 2018 and 2019. Four hfs lines of the OH 18 cm transitions were observed with the L-Band receiver. The beam size (FWHM) is $470''$, where the beam efficiency is 82%. A typical system temperature was from 18 to 29 K. The resolution of the backend correlator was tuned to be 0.26 kHz, corresponding to the velocity resolution of 0.047 km s^{-1} at 1.65 GHz. The integration time was about 1.5 hours/position. Such a long integration time was necessary to obtain an rms noise temperature of $\sim 10 \text{ mK}$ at a velocity resolution of 0.2 km s^{-1} .

The observations were conducted toward the positions indicated by the yellow circles arranged in the three strips shown in Figure 2. The reference $(0', 0')$ positions of strip-1 and strip-2 are $(\alpha_{2000}, \delta_{2000}) = (17^{\text{h}}20^{\text{m}}49^{\text{s}}.0, -26^{\circ}53'8.0'')$ and $(17^{\text{h}}27^{\text{m}}12^{\text{s}}.0, -26^{\circ}42'59.0'')$, respectively. The observations along strip-1 are arranged to assess the impact of UV heating from θ -Oph by determining the gas kinetic temperature as a function of the distance from the star. The strip-2 is parallel to the W-E filament seen in the visual extinction (A_K) map (Figure 1) and the ^{13}CO map (cyan contours in Figure 2). With the observation along strip-2, we examine whether the material at the interface of the W-E and S-N filaments has an increased temperature. Strip-3 is perpendicular to strip-2 and is centered on a position located on the interface of the filaments, i.e. at the offset of $(32', 0')$ in strip-2.

Intensities of the radio continuum background emission are evaluated for each observed position from the HIPASS 1.4 GHz continuum data (Calabretta et al. 2014) by following the method of Tang et al. (2017). The intensities along strip-1 and strip-2 are found to be $\sim 4.5\text{--}4.9 \text{ K}$ and $\sim 5.1\text{--}5.8 \text{ K}$ at 1667 MHz, respectively, and tend to be higher toward the Galactic center direction.

3. RESULT

Figure 3 shows the spectra of the OH 18 cm transition observed along strip-1 (Figure 2). The 1612 MHz line shows a clear absorption feature for all the observed positions. In contrast, the 1720 MHz line shows a brighter emission than expected for the LTE condition (see Section 1). This trend is the same as that seen in warm diffuse clouds (Ebisawa et al. 2015). Hence, we are looking at a warm ($>$

40 K) gas component of the Pipe nebula in the OH 18 cm transition. The 1665 and 1667 MHz lines are the strongest at the central position, and they become weaker to cloud peripheries. The peak intensity, the line width, and the LSR velocity are derived by fitting the Gaussian function to each observed spectrum, where the line width and the LSR velocities are assumed to be identical among the hyperfine components. The results are summarized in Table 1. The average LSR velocity of 3.3 km s⁻¹ is shown by blue dotted lines in Figure 3. This LSR velocity is consistent with that reported by Onishi et al. (1999).

Figures 4 and 5 show the spectra of the OH 18 cm transition observed along strip-2 (Figure 2) in the stem ($\Delta\alpha = -16', -8', 0', 8', 16', 24'$) and bowl ($\Delta\alpha = 32', 40', 48', 56', 64', 72', 80'$) regions, respectively. Toward the stem region (Figure 4), the absorption in the 1612 MHz line and the enhanced emission of the 1720 MHz line are observed, as is the case for strip-1 (Figure 3). The main lines (1665 and 1667 MHz) are observed in emission at V_{LSR} of (3.5 – 4.0) km s⁻¹ in this region, except for the (+24', 0') position. However, the main lines sharply turn from emission to absorption around the boundary between the stem region and the bowl region. This sharp change is apparent by comparing the spectra at the (+16', 0') and (+24', 0') positions. Namely, the main lines show emission at the (+16', 0') position, whereas clear absorption features of these lines are seen in the (+24', 0') position. Absorption in the main lines is present in almost all the observed positions in the bowl region (Figure 5). It should be noted that the radio continuum background emission in the bowl region is brighter than that in the stem region (Calabretta et al. 2014), which might explain the absorption of the main lines in the bowl region. However, the contribution of the background emission cannot fully explain the sharp transition from emission to absorption of the main lines at the interface of filaments around (24', 0') or (32', 0') positions. Later, in Section 5, we argue that a rise in the gas kinetic temperature produces the absorption at the interface.

In addition, several positions in the bowl region ($\Delta\alpha = 56', 64'$ (marginal), 72') have a velocity component ($V_{\text{LSR}} \sim (5 - 6)$ km s⁻¹) that shows the absorption in the 1720 MHz line. According to Ebisawa et al. (2019), the 1720 MHz absorption traces relatively cold ($T_k < 30$ K) gas with high OH column density ($> 10^{15}$ cm⁻²) illuminated by FIR radiation from dust grains in a surrounding warm

cloud. The positions showing the above characteristics are indeed located in the inner part of the S-N filament (Figure 2). This suggests that the component showing the 1720 MHz absorption represents a relatively cold part of the filament. In addition, the 1720 MHz absorption feature is seen only in the eastern positions of the bowl region. According to the archival IRAS and Herschel continuum maps, the dust temperature is higher toward the eastern part of strip-2. Since FIR radiation at the wavelengths of the 53 and 35 μm plays an important role in causing the 1720 MHz absorption (Ebisawa et al. 2019), the FIR pumping effect becomes more efficient with a higher dust temperature of the surrounding cloud. This qualitatively explains the appearance of the 1720 MHz absorption in the eastern part.

As shown in Figure 4, the four hfs components of the OH 18 cm transition show two velocity components in the stem region at V_{LSR} of ~ 3.0 and ~ 4.0 km s^{-1} (blue and red dotted lines, respectively). In contrast, the 3 km s^{-1} component is generally faint or almost absent in the bowl region (Figure 5). whereas the ~ 4.0 and ~ 5.0 – 6.0 km s^{-1} components are observed there. The line parameters for the two velocity components in the stem and bowl regions are determined by fitting the double Gaussian function to the observed spectra of the four hyperfine components except for the (24, 0), (32, 0), (40, 0), and (72, 0) positions, where the line width and the LSR velocity are assumed to be identical among the hyperfine components. For the (24,0) and (32,0) positions, which correspond to the interface of the W-E and S-N filaments, we cannot determine the line parameters assuming two velocity components due to heavy blending. Hence, the line parameters are determined by the single Gaussian fit. For the (72, 0) position, we employ the triple Gaussian fitting. On the other hand, the spectrum of the (40, 0) position is so complicated that we cannot fit the hyperfine structure in any way. The obtained line parameters are summarized in Table 2.

Figure 6 shows the spectra of the OH 18 cm transition observed along strip-3 (Figure 2). The main lines appear in absorption at all the observed positions. The two velocity components at $V_{\text{LSR}} \sim 3$ and 4 km s^{-1} are clearly seen toward the southern positions (32', -8') and (32', -16'), whereas they are blended in the (32', 0') position. As for the (32', 8') position, the two components (4.16 and

5.84 km s⁻¹) are seen. The double Gaussian fit is applied to strip-3 positions except for the (32', 0') position. The obtained line parameters are summarized in Table 3.

4. HEATING EFFECT FROM θ -OPHIUCHI

We perform a least-square fit on the hfs intensities derived above to determine the gas kinetic temperature and the OH column density for all the observed positions along strip-1 (Figure 2) by using the statistical equilibrium calculation described by [Ebisawa et al. \(2015\)](#). Here, we assume an H₂ column density of 10³ cm⁻³ and an H₂ ortho-to-para ratio of 3 (Table 4). Since the hfs intensities of the OH 18 cm transition are insensitive to an H₂ density from 10² cm⁻³ to 10⁶ cm⁻³ ([Ebisawa et al. 2015](#)), the assumption of an H₂ density of 10³ cm⁻³ is just arbitrary, and does not affect the results. Here, the intensity of the background continuum emission is evaluated from the HIPASS 1.4 GHz continuum data ([Calabretta et al. 2014](#)), as mentioned in Section 2. The effects of the FIR radiation and the line overlap are not included in this calculation. The collisional rate coefficients of OH reported by [Offer et al. \(1994\)](#) are employed in the calculations. In this analysis, the hfs intensities including the 1612 MHz absorption are well reproduced, and the gas kinetic temperature and the OH column density at each position are determined.

Figure 7 shows the derived gas kinetic temperatures as a function of the angular offset along strip-1 (Figure 1), where the star θ -Ophiuchi is closer to the northeastern positions on the plane of the sky. The gas temperature is found to be slightly higher at the cloud peripheries than at the cloud center along the strip 1. Since the strip 1 is well apart from the interaction region between the stem and bowl structure, the main heating mechanism is likely the UV heating. Here, we qualitatively discuss its effect on strip 1. According to [Onishi et al. \(1999\)](#), the peak H₂ column density is 8.5×10^{21} cm⁻², which corresponds to the visual extinction of about 8.5. However, the cloud peripheries are illuminated by external UV radiation, and enhancement of the gas kinetic temperature there is expected by photodissociation region (PDR) models (e.g., [Tielens & Hollenbach 1985](#); [Spaans 1996](#)). Such a PDR effect is indeed reported for the ρ -Oph cloud in the OH 18 cm transition ([Ebisawa et al. 2015](#)). Hence, the above temperature structure can be understood in terms of the external UV radiation effect. On the other hand, we find no temperature gradient as a function of the

apparent distance from θ -Oph. This result suggests that the heating effect from θ -Oph is not seen in the observed temperature structure. Hence, the heating source would likely be the interstellar UV radiation. It should be noted, however, that we also expect no temperature gradient along the E-W direction due to the illumination by θ -Oph, if θ -Oph is illuminating the observed filament from the back side or the front side.

5. THE MECHANISM CAUSING ABSORPTION IN THE MAIN LINES

In this section, we explore the origin of the absorption observed in the main OH hfs lines (1665 and 1667 MHz) of the OH 18 cm transition, which is observed in the bowl region of the Pipe nebula (Figures 4 and 5). The absorption is exclusively observed in the bowl region where these filaments overlap, and it starts to appear from the interface of the filaments (i.e. $(24', 0')$ position) to the bowl region. Hence, the main line absorption might be related to the interaction between the W-E and S-N filaments.

Figure 8 shows the intensities of the four hfs lines of the OH 18 cm transition as a function of the gas kinetic temperature, which are derived by using the statistical equilibrium calculation (Ebisawa et al. 2015). The H_2 density, the H_2 ortho-to-para ratio, the OH column density and the intensity of the radio continuum background emission are assumed to be 10^3 cm^{-3} , 3, 10^{14} cm^{-2} and 5 K, respectively. No effect of the FIR radiation is included. The 1665 and 1667 MHz lines appear in absorption with a gas kinetic temperature higher than about 60 K. The absorption becomes deeper for a higher gas kinetic temperature. This prediction suggests that the absorption of the main lines observed in the bowl region traces warm gas with a gas kinetic temperature higher than 60 K. It should be noted that the fainter the continuum background temperature, the higher a gas kinetic temperature is required to reproduce the absorption. If the cosmic microwave background (2.73 K) were to provide the continuum background, a gas kinetic temperature higher than about 100 K would be necessary to reproduce the absorption.

Absorption in the 18 cm main hfs lines of OH can qualitatively be explained in terms of the following non-LTE effect. Most of the OH molecules excited to the rotationally excited states in the $^2\Pi_{3/2}$ ladder ($J = 5/2, 7/2$ or higher) by collisions with H_2 molecules are quickly de-excited to the ground

rotational state (${}^2\Pi_{3/2} J = 3/2$) through rotational transitions within the ${}^2\Pi_{3/2}$ ladder (red downward arrows in Figure 9). During the radiative decay, the Λ -type transitions within each rotational level can occur, as represented by the blue and green arrows in Figure 9. Thus the populations of the lower Λ -type doubling levels relative to those of the upper levels are slightly increased in the ${}^2\Pi_{3/2} J = 5/2, 7/2$, and higher states, as represented by the red ellipses in Figure 9. These overpopulations in the lower Λ -type doubling levels subsequently produce a similar anomaly in the ground rotational state via rotational transitions within the ${}^2\Pi_{3/2}$ ladder (red downward arrows in Figure 9). In this situation, the excitation temperatures of the 1665 and 1667 MHz lines are decreased, which causes absorption against the background radiation.

It should be noted that the Λ -type transitions in the rotationally excited states rarely occur compared to the rotational transitions, since Einstein's A coefficients of these transitions are about 10^9 – 10^{10} times lower than those of the rotational transitions (Offer et al. 1994). This suggests that the Λ -type transitions in the rotationally excited states affect the populations only slightly. Nevertheless, such a slight effect on the population can significantly change the excitation temperature of the OH 18 cm transition because of the small energy gap between the Λ -type doubling levels ($\Delta E \sim 0.08$ K). This energy gap is so small that the populations of the upper and lower states of this transition are almost comparable even in the low temperature. For example, assuming an excitation temperature of 2 K, 10 K and 100 K, the population difference between the upper and lower states are about 2%, 0.4% and 0.04%, respectively. This implies that the excitation temperature can be lower than the continuum temperature, just by raising the lower state population by only one percent or less, which would be possible through the Λ -type transitions. Collisional excitation to the upper rotationally excited states becomes more efficient with increasing gas kinetic temperature, which leads to deeper absorption features of the main lines, as shown in Figure 8. Note that the contributions from the ${}^2\Pi_{1/2}$ state are not important, because inter-ladder radiative transitions from ${}^2\Pi_{1/2}$ to ${}^2\Pi_{3/2}$ are less frequent than those within the ${}^2\Pi_{1/2}$ or ${}^2\Pi_{3/2}$ ladder.

Figure 10 shows the expected intensities of the hfs lines of the OH 18 cm transition derived from our statistical equilibrium calculations as a function of the H_2 density. Here, the OH column density,

the gas kinetic temperature, and the H₂ ortho-to-para ratio are assumed to be 10¹⁴ cm⁻², 75 K and 3, respectively. The intensity of the radio continuum background emission is assumed to be 5 K as a representative value. The absorption features of the main lines as well as of the 1612 MHz line are reproduced in the H₂ density range from 1 to 10⁶ cm⁻³. Moreover, intensities of all the four hfs lines are insensitive to the H₂ density from 10² to 10⁶ cm⁻³, as was found in our previous paper (Ebisawa et al. 2015). This suggests that the radiative transitions are dominant over the collisional transitions at this H₂ density range for a gas kinetic temperature of 75 K. This is consistent with the above picture on the origin of the main lines absorption, where the absorption is essentially produced by the Λ -type transitions in the rotationally excited states during the rotational cascade.

In order to examine if our statistical equilibrium analysis can quantitatively reproduce the absorption feature in the main lines as well as the intensities of the 1612 and 1720 MHz satellite lines, we first perform a least-squares fit on the intensities of the OH spectra observed on (+32', 0') position (Figure 11), which shows the deepest absorption feature. In this analysis, we conduct the same statistical equilibrium calculation as that used in Section 4, assuming an H₂ density of 10³ cm⁻³ and an H₂ ortho-to-para ratio of 3. As a result, the observed intensities of the four hfs lines are well reproduced by the simultaneous fit, as shown in the red lines in Figure 11. The gas kinetic temperature and the OH column density are determined to be 73.6 ± 0.8 K and (5.3 ± 0.2) × 10¹³ cm⁻², respectively. The gas kinetic temperature of 73.6 K is apparently higher than that derived in the stem region along strip-1 (40–60 K) (Figure 7).

6. ENHANCED TEMPERATURE IN THE INTERACTING REGION

We then perform the same least-squares fit on the hfs intensities of all the spectra along strip-2 (Figures 4 and 5) with our statistical equilibrium calculations. The density and the ortho-to-para ratio of H₂ are assumed to be 10³ cm⁻³ and 3, respectively in the fit. An effect of the FIR radiation is ignored, and hence, the fitting is not conducted for the velocity components showing the 1720 MHz absorption or its faint emission, that is the ~5.0 km s⁻¹ component of the (48', 0'), (56', 0') and (64', 0') positions, as well as the 5.7 km s⁻¹ component of the (72', 0') position. As presented by Ebisawa et al. (2019), accurate information on the FIR field and the cloud structure are necessary

to analyze the 1720 MHz absorption. Due to the lack of the information for the Pipe nebula, we exclude these components from the present analysis. In addition, the gas kinetic temperature cannot be determined for the (80', 0') position, because of poor signal-to-noise ratios of the satellite lines.

The derived gas kinetic temperatures and OH column densities are summarized in Table 5. Figure 12 shows the gas kinetic temperatures as a function of the angular offset in right ascension from the (0', 0') position. As for the stem region (right five points in Figure 12), the temperatures of the ~ 3 and ~ 4 km s⁻¹ components are determined to be about 40–60 K, as represented by blue and red colors, respectively. The temperature is slightly increased at the (24', 0') position, and reaches the highest value of 73.6 ± 0.8 K at the interface of the stem and bowl regions. (i.e. the (32', 0') position). Note that the quoted errors do not include the systematic uncertainty due to the collisional rates, radiative transfer effects, and the fact that we are neglecting the FIR radiation and line overlap. Toward the eastern positions in the bowl region (left four points in Figure 12), the gas kinetic temperatures are determined to be 50–60 K, which are comparable to those determined for the stem region ($\Delta\alpha = -16'-16'$). As shown in Figure 12, the derived gas kinetic temperature is indeed highest at the positions located on the interface of the two filamentary structures (Figure 2) ($\Delta\alpha = 24', 32'$) (Figure 2). The rise of the gas kinetic temperature can be interpreted as the effect of heating caused by the collisions between the filaments.

Similar least-square analyses for the hfs intensities are performed for the spectra observed along strip-3, as shown in Figure 13. The results are summarized in Table 6. Gas kinetic temperatures of the ~ 4 km s⁻¹ component are about 70 K for the four positions, whereas they are ~ 60 K for the ~ 3 and 5 km s⁻¹ components. Since all these positions are located at the interface of the filaments (Figure 2), the high gas kinetic temperature (~ 70 K) compared to the western and eastern positions on strip-2 (~ 50 –60 K) further supports the existence of the filament-filament collision.

When the collision velocity is assumed to be the velocity difference between the stem and bowl region (~ 1.5 km s⁻¹), the kinetic energy released by the collision is estimated to be $\sim 10^{-10}$ erg cm⁻³, where the H₂ density of 10³ cm⁻³ is arbitrarily assumed. This can be balanced by the cooling rate by Goldsmith & Langer (1978), and the equilibrium temperature is roughly estimated to be

100 K. Here, we assume the cooling time of 10^4 year according to [Inoue & Inutsuka \(2012\)](#). This temperature is comparable with that observed in the interacting region. Thus, this rough estimate implies that the slight temperature enhancement is possible in the interacting region.

Warm gas with a temperature of 74 K, heated by the filament-filament collision, is cooled down mainly by rotational line emission of CO for an H_2 density of 10^3 cm^{-3} ([Inoue & Inutsuka 2012](#)). As mentioned above, the cooling time (t_{cool}) is estimated to be around 10^4 year according to [Koyama & Inutsuka \(2000\)](#) with a cooling rate of $10^{-26} \text{ erg cm}^{-3} \text{ s}^{-1}$ ([Inoue & Inutsuka 2012](#)). Assuming that this warm gas expands with a constant velocity of 1.5 km s^{-1} , which corresponds to the typical velocity difference between the blue-shifted and red-shifted components of the Pipe nebula of 3.0 km s^{-1} and $4\text{--}5 \text{ km s}^{-1}$, respectively, the gas can extend in space by about 0.015 pc within the cooling time. This length corresponds to a typical spatial scale of a shocked warm region, and hence we hereafter denote it as L_{warm} ($= 0.015 \text{ pc}$). On the other hand, the extent of the cloud along the line-of-sight (L_{LOS}) can roughly be estimated from the H_2 density ($n(H_2)$), the OH column density ($N(\text{OH})$) and the OH fractional abundance ($X(\text{OH})$) relative to H_2 with the following equation:

$$L_{\text{LOS}} = \frac{N(\text{OH})}{X(\text{OH})n(H_2)}. \quad (1)$$

We employ an H_2 density of 10^3 cm^{-3} and an OH column density of $5.3 \times 10^{13} \text{ cm}^{-2}$, a latter of which is determined for the $(0', 32')$ position (Table 5). Assuming an OH abundance of 10^{-7} , which is a typical value in diffuse clouds ([Wiesemeyer et al. 2012](#)), L_{LOS} is estimated to be $\sim 0.2 \text{ pc}$. If the OH fractional abundance is one order of magnitude higher ($X(\text{OH}) = 10^{-6}$), which could be possible in a shocked gas according to [Draine & Katz \(1986\)](#), L_{LOS} could be 0.01 pc . The latter value ($L_{\text{LOS}} \sim 0.02 \text{ pc}$) for the shocked gas case ($X(\text{OH})=10^{-6}$) is comparable to the L_{warm} of 0.015 pc . This result suggests the presence of shock-induced compression at the interface of the two filaments, and supports the filament-filament collisions picture in the Pipe nebula.

7. SUMMARY

We have observed the four hfs components of the OH 18 cm transitions toward the Pipe nebula along the two strip lines and determined the gas kinetic temperatures accurately. Along strip-1, the

gas kinetic temperature is found to have no relation to the apparent distance to the nearby star, θ -Oph. This result suggests that the heating effect from θ -Oph does not significantly contribute to the heating of the Pipe nebula, although a possibility that θ -Oph illuminates the cloud from the front side or the back side in the 3D configuration remains. On strip-2 and strip-3, the absorption feature of the 1665 and 1667 MHz main lines is observed in the bowl region, and the deepest absorption is observed just at the interface of the W-E and S-N filamentary structures. Our statistical equilibrium calculations successfully reproduce this absorption feature with a gas kinetic temperature higher than ~ 60 K, where an increasing gas kinetic temperature would deepen the absorption. The derived temperature is indeed the highest at the interface of the filaments, indicating shock heating at the filament interface. This observation demonstrates a unique characteristic of the OH 18 cm transition as a new tool to study the molecular-cloud formation.

The authors thank the anonymous reviewer for valuable comments. The authors are grateful to the staff of the Green Bank Telescope for excellent support. This study is financially supported by Grant-in-Aid from Ministry of Education Sports, Science, and Technologies of Japan (25400223, 18H05222, 19H05069, and 19K14753).

REFERENCES

- Alves, F. O., & Franco, G. A. P. 2007, *A&A*, 470, 597, doi: [10.1051/0004-6361:20066759](https://doi.org/10.1051/0004-6361:20066759)
- Alves, F. O., Franco, G. A. P., & Girart, J. M. 2008, *A&A*, 486, L13, doi: [10.1051/0004-6361:200810091](https://doi.org/10.1051/0004-6361:200810091)
- Alves, F. O., Frau, P., Girart, J. M., et al. 2014, *A&A*, 569, L1, doi: [10.1051/0004-6361/201424678](https://doi.org/10.1051/0004-6361/201424678)
- Calabretta, M. R., Staveley-Smith, L., & Barnes, D. G. 2014, *PASA*, 31, e007, doi: [10.1017/pasa.2013.36](https://doi.org/10.1017/pasa.2013.36)
- Caswell, J. L. 2004, *MNRAS*, 349, 99, doi: [10.1111/j.1365-2966.2004.07472.x](https://doi.org/10.1111/j.1365-2966.2004.07472.x)
- Darling, J., & Giovanelli, R. 2002, *AJ*, 124, 100, doi: [10.1086/341166](https://doi.org/10.1086/341166)
- Draine, B. T., & Katz, N. 1986, *ApJ*, 306, 655, doi: [10.1086/164375](https://doi.org/10.1086/164375)
- Ebisawa, Y., Inokuma, H., Sakai, N., et al. 2015, *ApJ*, 815, 13, doi: [10.1088/0004-637X/815/1/13](https://doi.org/10.1088/0004-637X/815/1/13)
- Ebisawa, Y., Sakai, N., Menten, K. M., & Yamamoto, S. 2019, *ApJ*, 871, 89, doi: [10.3847/1538-4357/aaf72b](https://doi.org/10.3847/1538-4357/aaf72b)
- Elitzur, M., Goldreich, P., & Scoville, N. 1976, *ApJ*, 205, 384, doi: [10.1086/154289](https://doi.org/10.1086/154289)
- Franco, G. A. P., Alves, F. O., & Girart, J. M. 2010, *ApJ*, 723, 146, doi: [10.1088/0004-637X/723/1/146](https://doi.org/10.1088/0004-637X/723/1/146)
- Frau, P., Girart, J. M., Alves, F. O., et al. 2015, *A&A*, 574, L6, doi: [10.1051/0004-6361/201425234](https://doi.org/10.1051/0004-6361/201425234)
- Goldsmith, P. F., & Langer, W. D. 1978, *ApJ*, 222, 881, doi: [10.1086/156206](https://doi.org/10.1086/156206)
- Gritschneider, M., & Lin, D. N. C. 2012, *ApJ*, 754, L13, doi: [10.1088/2041-8205/754/1/L13](https://doi.org/10.1088/2041-8205/754/1/L13)
- Harju, J., Winnberg, A., & Wouterloot, J. G. A. 2000, *A&A*, 353, 1065
- Hoffman, I. M., Goss, W. M., Brogan, C. L., & Claussen, M. J. 2005, *ApJ*, 620, 257, doi: [10.1086/427018](https://doi.org/10.1086/427018)
- Inoue, T., & Inutsuka, S.-i. 2012, *ApJ*, 759, 35, doi: [10.1088/0004-637X/759/1/35](https://doi.org/10.1088/0004-637X/759/1/35)
- Koyama, H., & Inutsuka, S.-I. 2000, *ApJ*, 532, 980, doi: [10.1086/308594](https://doi.org/10.1086/308594)
- Lada, C. J., Muench, A. A., Rathborne, J., Alves, J. F., & Lombardi, M. 2008, *ApJ*, 672, 410, doi: [10.1086/523837](https://doi.org/10.1086/523837)
- Li, D., Tang, N., Nguyen, H., et al. 2018, *ApJS*, 235, 1, doi: [10.3847/1538-4365/aaa762](https://doi.org/10.3847/1538-4365/aaa762)
- Lombardi, M., Alves, J., & Lada, C. J. 2006, *A&A*, 454, 781, doi: [10.1051/0004-6361:20042474](https://doi.org/10.1051/0004-6361:20042474)
- Offer, A. R., van Hemert, M. C., & van Dishoeck, E. F. 1994, *J. Chem. Phys.*, 100, 362, doi: [10.1063/1.466950](https://doi.org/10.1063/1.466950)
- Onishi, T., Kawamura, A., Abe, R., et al. 1999, *PASJ*, 51, 871, doi: [10.1093/pasj/51.6.871](https://doi.org/10.1093/pasj/51.6.871)
- Román-Zúñiga, C. G., Alves, J. F., Lada, C. J., & Lombardi, M. 2010, *ApJ*, 725, 2232, doi: [10.1088/0004-637X/725/2/2232](https://doi.org/10.1088/0004-637X/725/2/2232)
- Spaans, M. 1996, *A&A*, 307, 271

- Tang, N., Li, D., Heiles, C., et al. 2017, ApJ, 839, 8, doi: [10.3847/1538-4357/aa67e9](https://doi.org/10.3847/1538-4357/aa67e9)
- Tielens, A. G. G. M., & Hollenbach, D. 1985, ApJ, 291, 722, doi: [10.1086/163111](https://doi.org/10.1086/163111)
- van Langevelde, H. J., van Dishoeck, E. F., Sevenster, M. N., & Israel, F. P. 1995, ApJ, 448, L123, doi: [10.1086/309613](https://doi.org/10.1086/309613)
- Wiesemeyer, H., Güsten, R., Heyminck, S., et al. 2012, A&A, 542, L7, doi: [10.1051/0004-6361/201218915](https://doi.org/10.1051/0004-6361/201218915)
- Wolak, P., Szymczak, M., & Gérard, E. 2012, A&A, 537, A5, doi: [10.1051/0004-6361/201117263](https://doi.org/10.1051/0004-6361/201117263)
- Xu, D., Li, D., Yue, N., & Goldsmith, P. F. 2016, ApJ, 819, 22, doi: [10.3847/0004-637X/819/1/22](https://doi.org/10.3847/0004-637X/819/1/22)

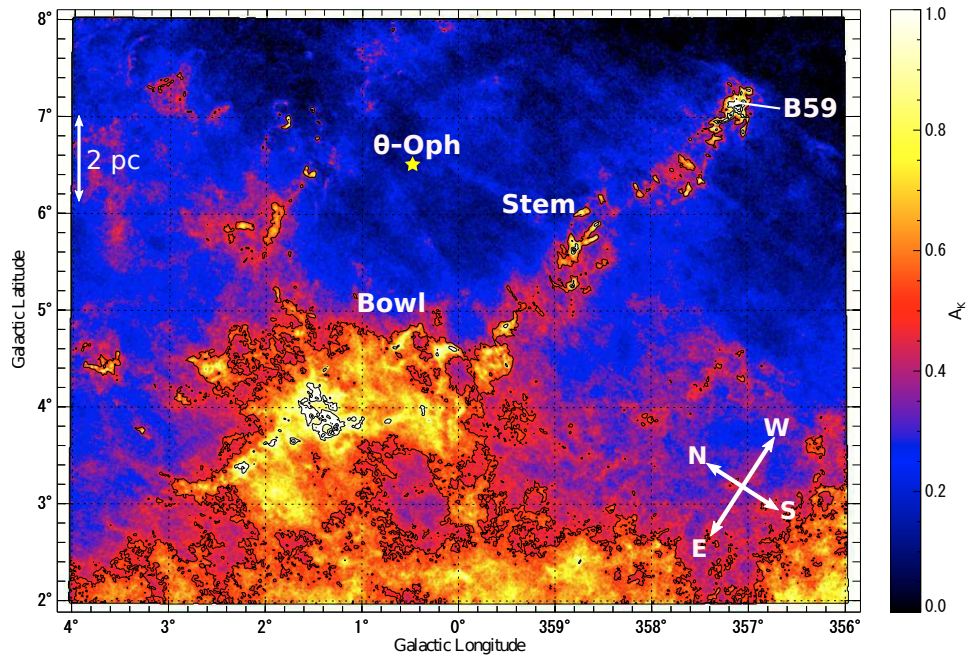


Figure 1. The visual extinction (A_k) map observed for the Pipe nebula (Lombardi et al. 2006). The position of the θ -Ophiuchi is represented by a yellow star mark.

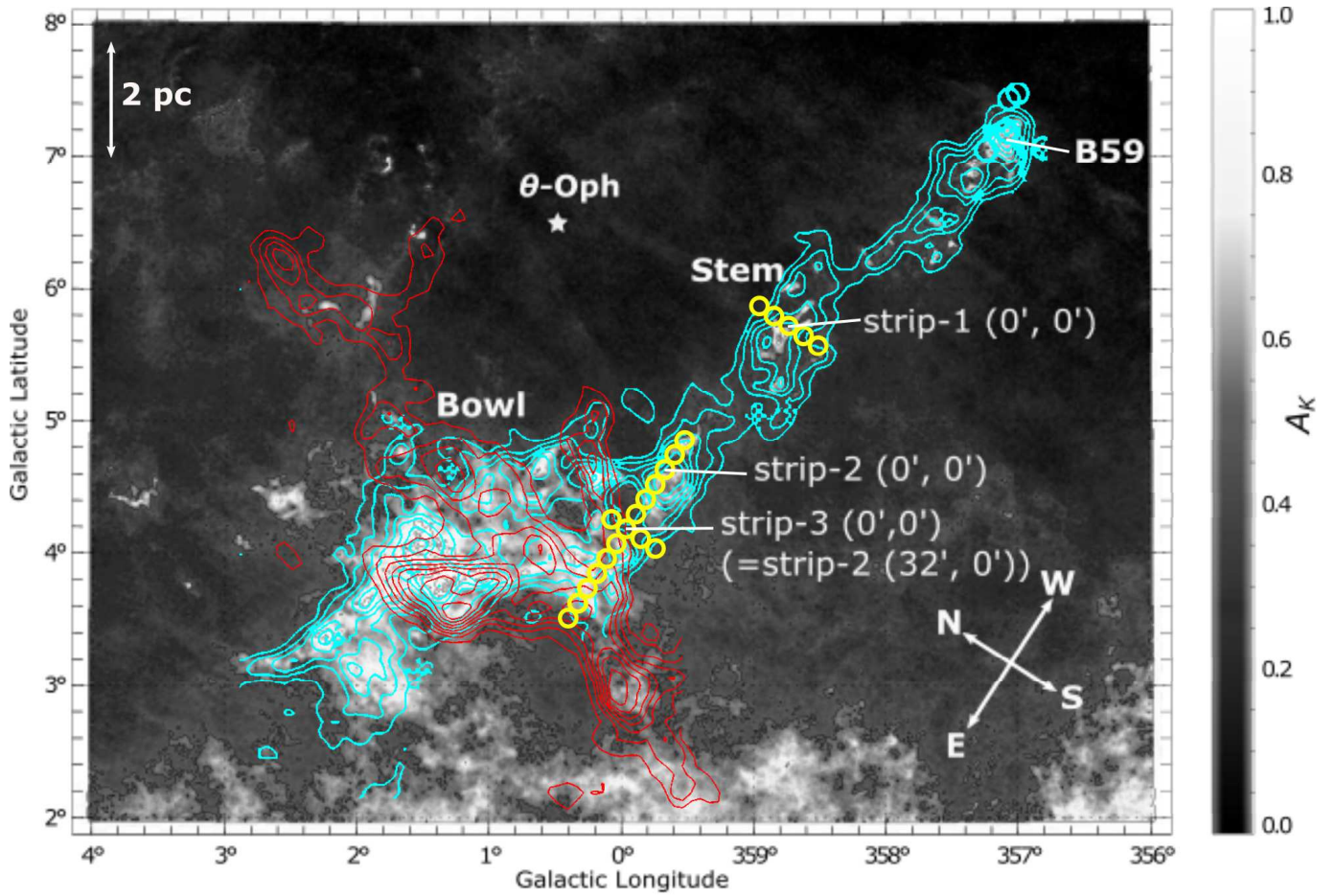


Figure 2. (Cyan) The integrated intensity map of the ^{13}CO ($J=1-0$) emission observed by Onishi et al. (1999). (Red) The integrated intensity map of the ^{12}CO ($J=1-0$) emission from 6 to 10 km s^{-1} observed by Onishi et al. (1999). (Gray) The visual extinction (A_k) map reported by Lombardi et al. (2006), which is the same as Figure 1. Yellow circles represent the observed positions in the OH 18 cm transition. A diameter of the circle corresponds to the HPBW beam size of the GBT of 8 arcmin.

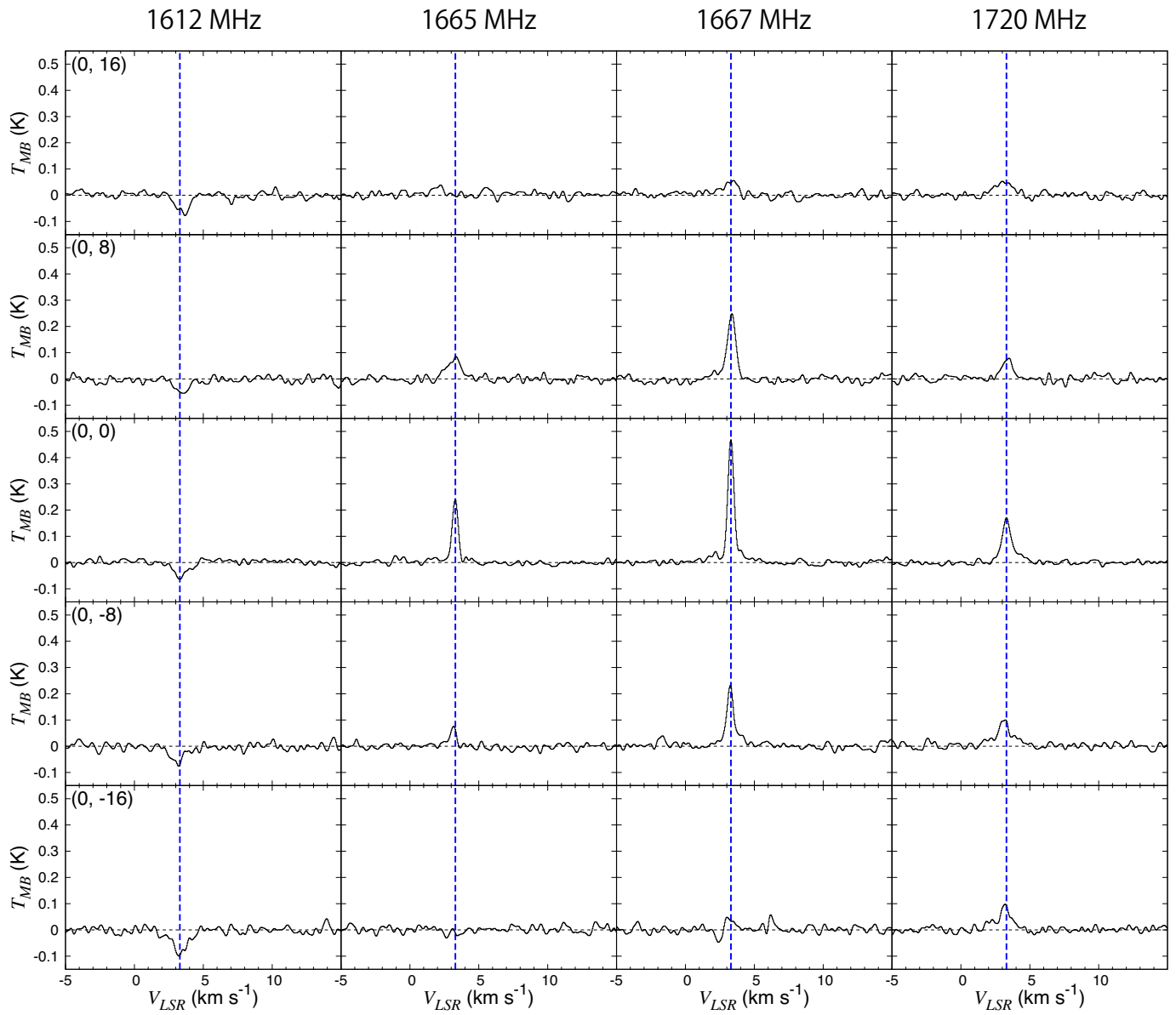


Figure 3. Spectra of the four hfs components of the OH 18 cm transition observed toward the Pipe nebula along strip-1 (Figure 2). The blue dotted lines represent the V_{LSR} of 3.3 km s^{-1} .

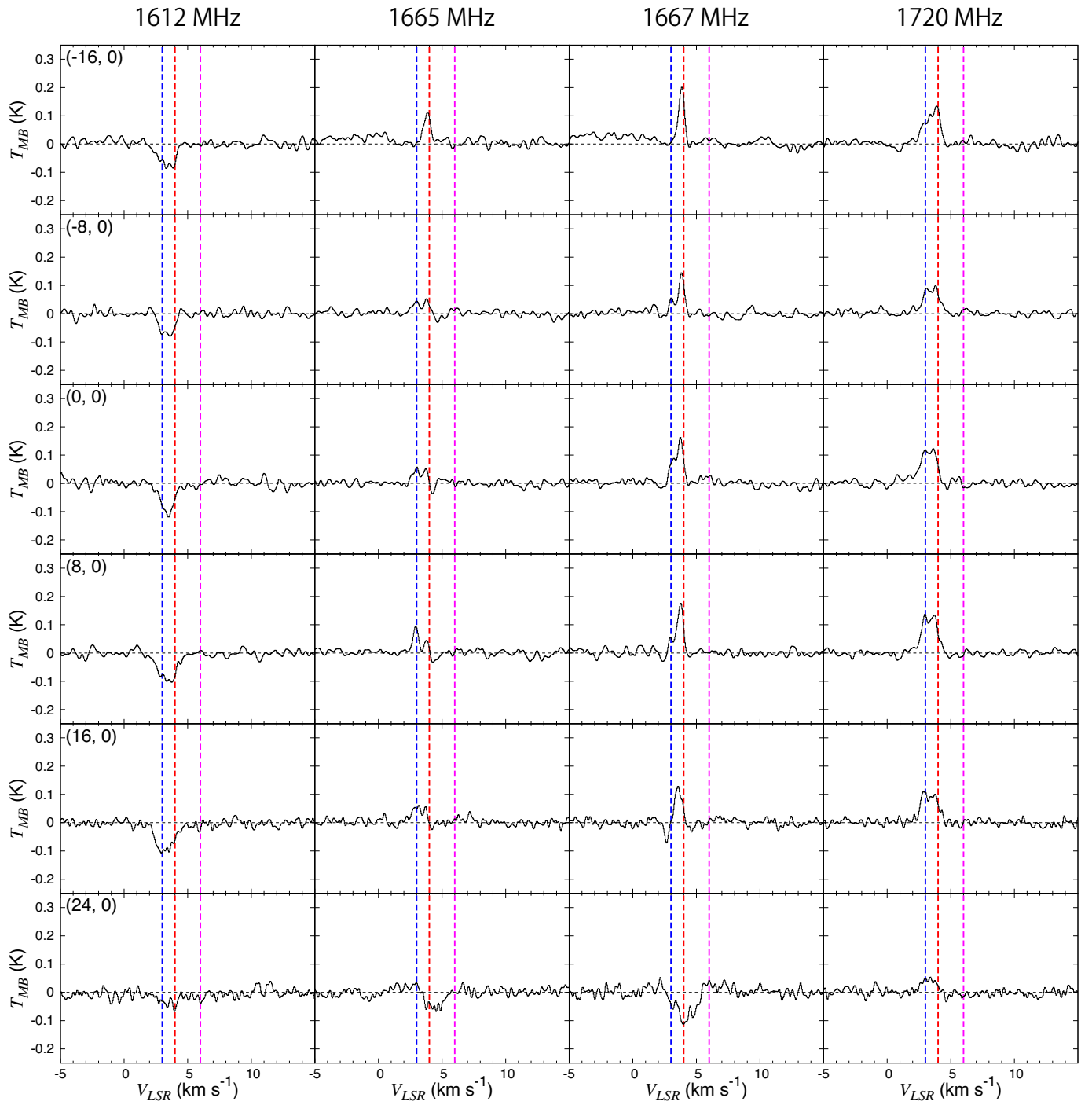


Figure 4. Spectra of the four hfs components of the OH 18 cm transition observed toward the stem region of the Pipe nebula along strip-2 (Figure 2). The blue, red and magenta dotted lines represent the V_{LSR} of 3.0, 4.0 and 6.0 km s^{-1} , respectively.

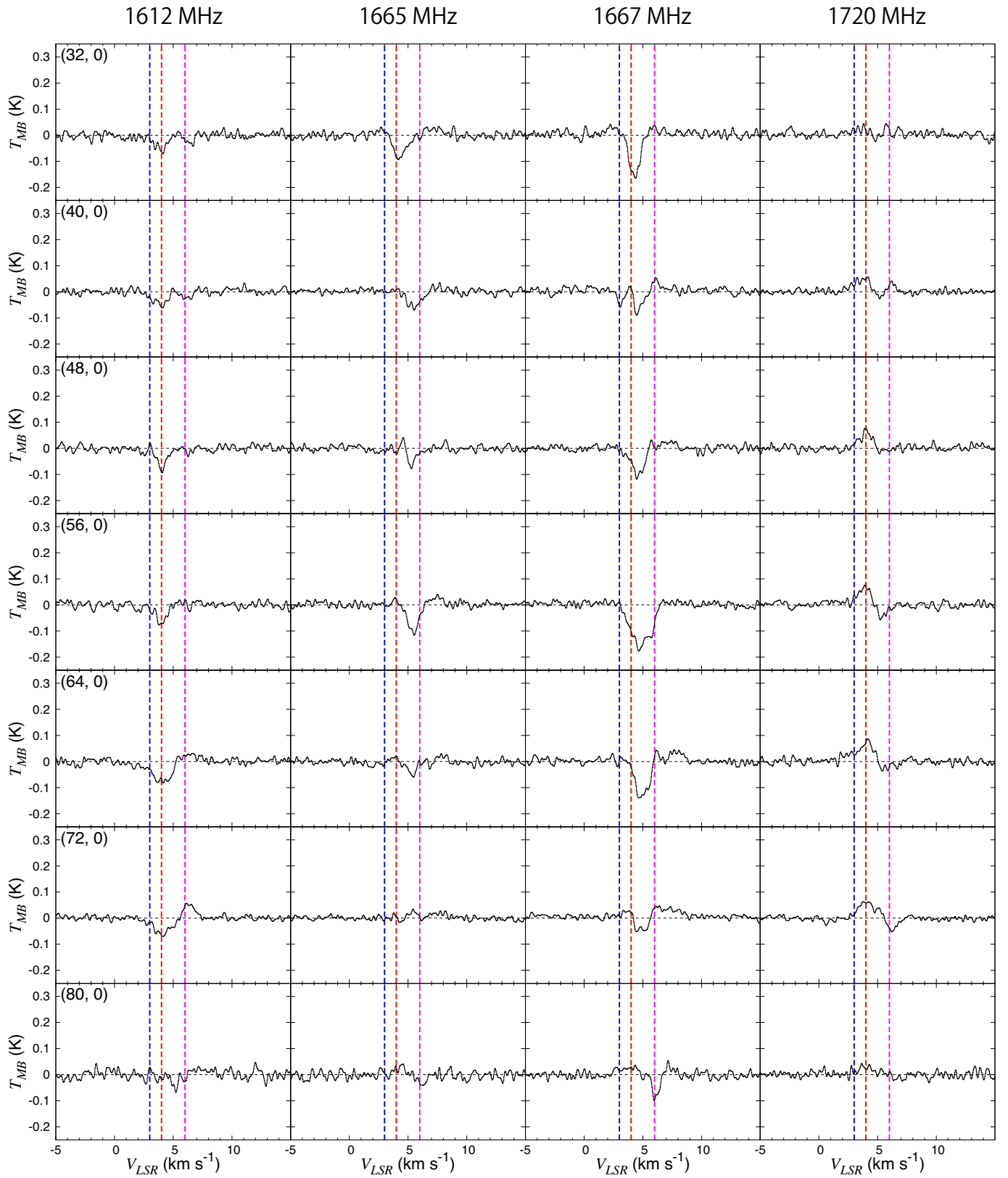


Figure 5. Spectra of the four hfs components of the OH 18 cm transition observed toward the bowl region of the Pipe nebula along strip-2 (Figure 2). The blue, red and magenta dotted lines represent the V_{LSR} of 3.0, 4.0 and 6.0 km s^{-1} , respectively.

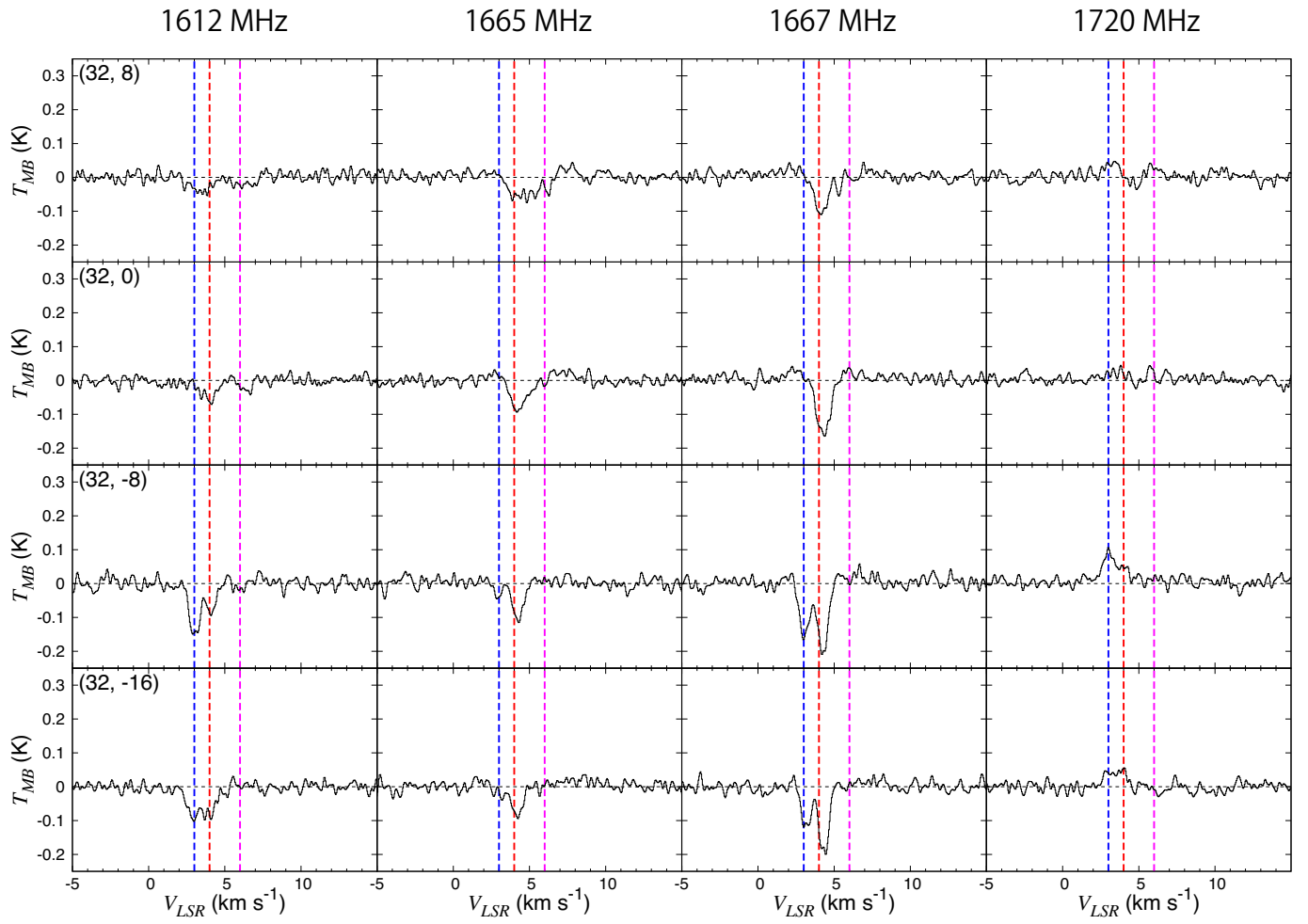


Figure 6. Spectra of the four hfs components of the OH 18 cm transition observed toward the Pipe nebula along strip-3 (Figure 2). The blue, red and magenta dotted lines represent the V_{LSR} of 3.0, 4.0 and 6.0 km s^{-1} , respectively.

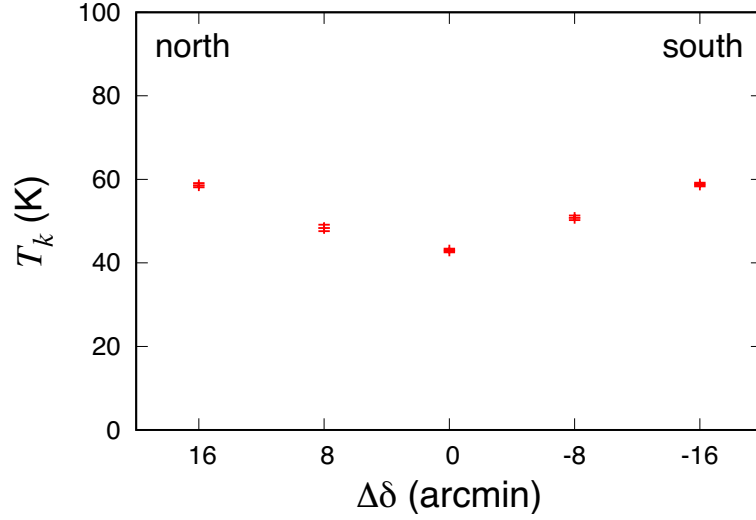


Figure 7. The gas kinetic temperatures along strip-1 (Figure 2) determined by using our statistical equilibrium calculations. The abscissa is the angular offset from the center (Table 1). Error bars denote three times the standard deviation.

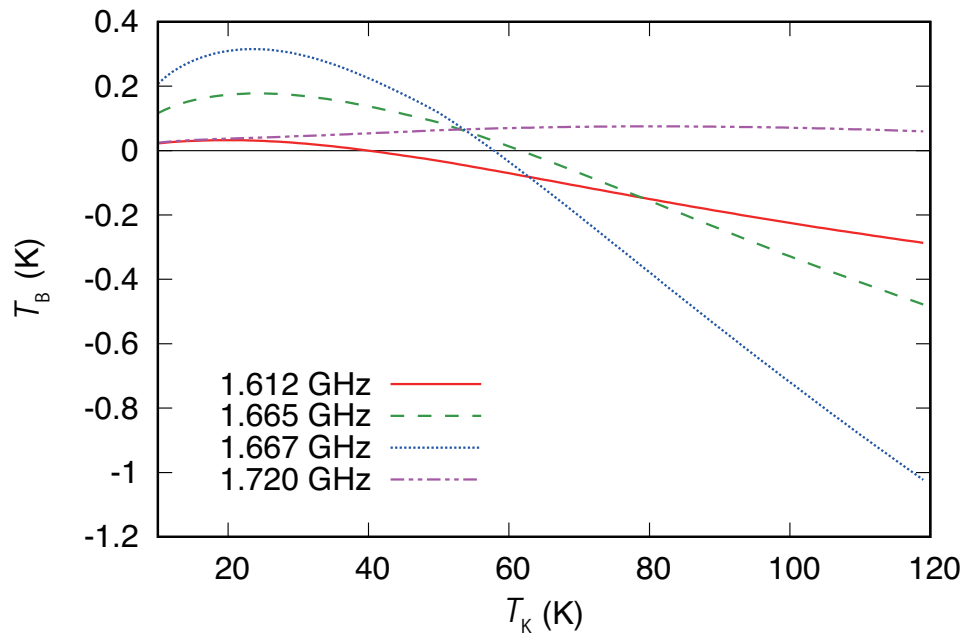


Figure 8. The derived intensities of the four hfs lines of the OH 18 cm transition as a function of the gas kinetic temperature, where the H_2 density, the OH column density, and the H_2 ortho-to-para ratio are assumed to be 10^3 cm^{-3} , 10^{14} cm^{-2} , and 3, respectively. The intensity of the radio continuum background emission is assumed to be 5 K.

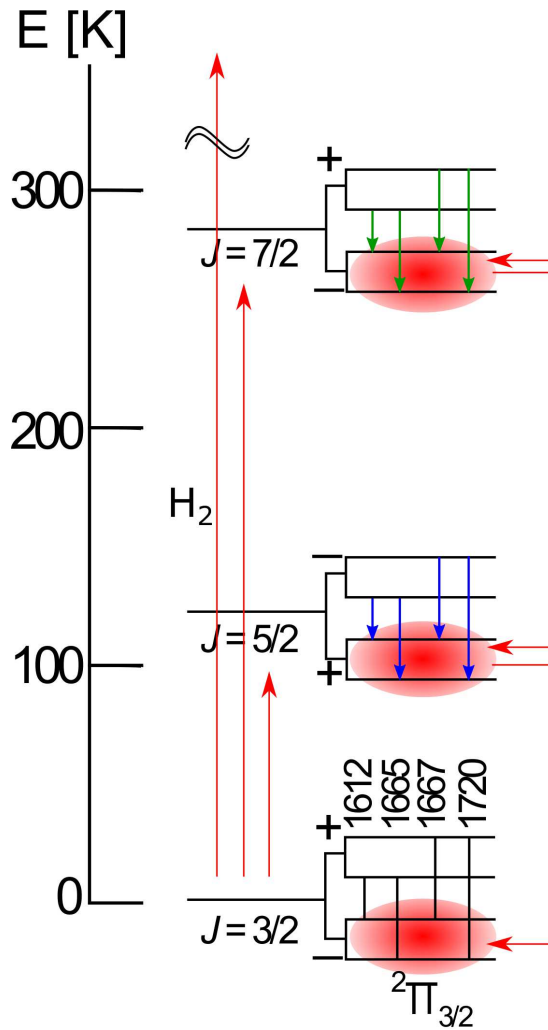


Figure 9. The rotational energy diagram for the $^2\Pi_{3/2}$ states of the OH molecule. The overpopulation in the lower Λ -type doubling levels of the rotationally excited states is produced by the Λ -type doubling transitions (green and blue arrows). The subsequent rotational transitions (red downward arrows) produce the overpopulations in the $-$ levels of the $J=3/2$ states, respectively.

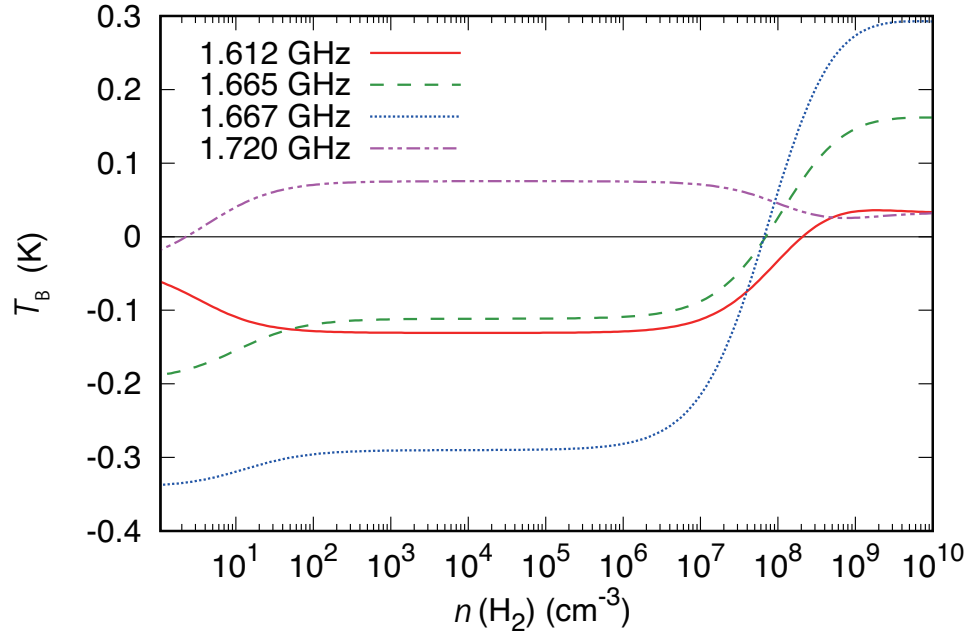


Figure 10. The derived intensities of the four hfs lines of the OH 18 cm transition as a function of the H₂ density, where the OH column density, the gas kinetic temperature, and the H₂ ortho-to-para ratio are assumed to be 10^{14} cm^{-2} , 75 K and 3, respectively. The intensity of the radio continuum background emission is assumed to be 5 K.

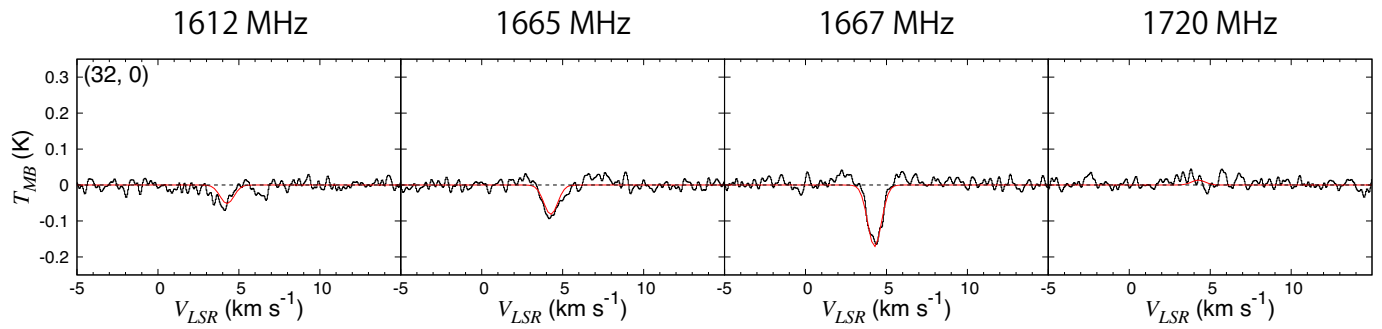


Figure 11. Spectra for the four hfs components of the OH 18 cm transition observed on the $(+32', 0')$ position on strip-2 (Figure 2). Red lines show the Gaussian profiles with the best-fit parameters derived from our statistical equilibrium calculations, namely the gas kinetic temperature of 73.6 ± 0.8 K and the OH column density of $(5.3 \pm 0.2) \times 10^{13} \text{ cm}^{-2}$.

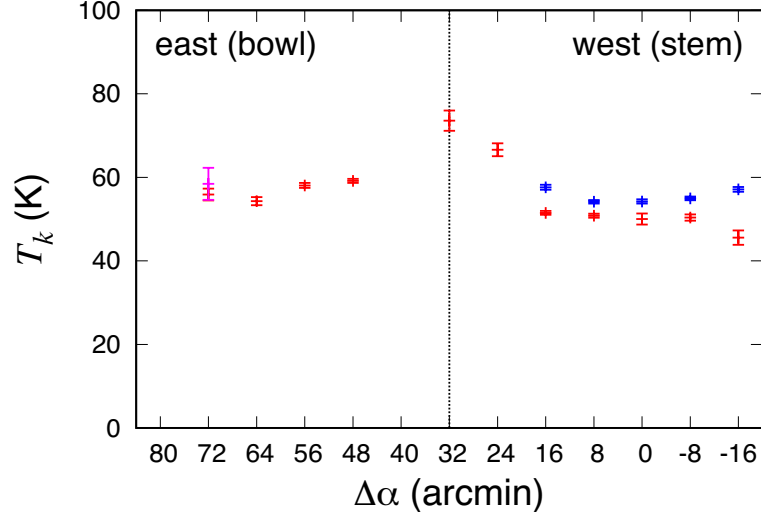


Figure 12. The gas kinetic temperatures along strip-2 in Figure 2 determined by using our statistical equilibrium calculations. The abscissa is the angular offset from the $(0', 0')$ position (Table 2). Error bars denote three times the standard deviation. The blue, red and magenta color represent the ~ 3 , ~ 4 , ~ 5 – 6 km s^{-1} velocity components, respectively.

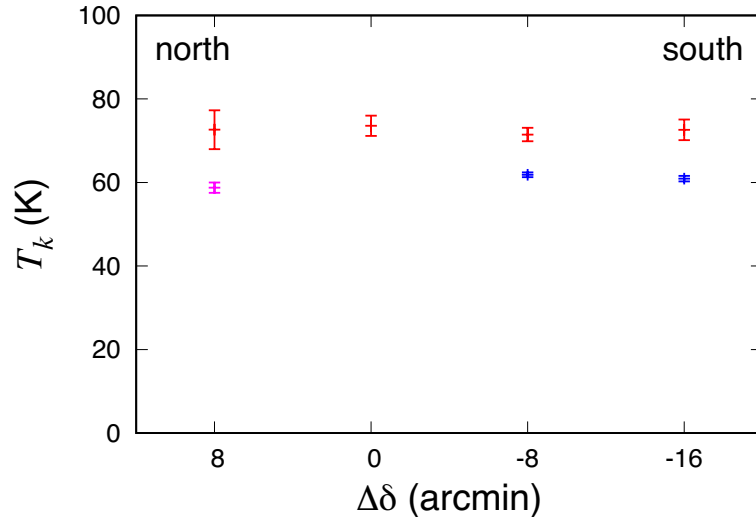


Figure 13. The gas kinetic temperatures along strip-3 in Figure 2 determined by using our statistical equilibrium calculations. The abscissa is the angular offset from the $(32', 0')$ position (Table 3). Error bars denote three times the standard deviation. The blue, red and magenta color represent the ~ 3 , ~ 4 , ~ 5 – 6 km s^{-1} velocity components, respectively.

Table 1. Observed line parameters toward the Pipe nebula along strip-1. ^a

$\Delta\delta$ (arcmin)	V_{LSR} (km s ⁻¹)	FWHM (km s ⁻¹)	T_{MB} (1612) (K)	T_{MB} (1665) (K)	T_{MB} (1667) (k)	T_{MB} (1720) (K)
-16	3.27 (2)	1.24 (4)	-0.092 (3)	-0.016 (3)	0.026 (3)	0.079 (3)
-8	3.216 (6)	0.82 (1)	-0.073 (3)	0.055 (3)	0.192 (3)	0.105 (3)
0	3.298 (2)	0.568 (4)	-0.074 (3)	0.226 (3)	0.450 (3)	0.188 (3)
8	3.336 (5)	0.82 (1)	-0.063 (3)	0.088 (3)	0.229 (3)	0.080 (3)
16	3.33 (2)	1.30 (4)	-0.061 (2)	0.005 (2)	0.051 (2)	0.053 (2)

^a $\Delta\delta$ in the first column denotes a Decl. offset from the $(\alpha_{2000}, \delta_{2000}) = (17^{\text{h}}20^{\text{m}}49^{\text{s}}.0, -26^{\circ}53'8.0'')$ position. The main beam temperatures (T_{MB}) of the four hfs lines of OH, the V_{LSR} value, and the linewidth (FWHM) are obtained by a Gaussian fit, assuming that the V_{LSR} values and the linewidths of the four hfs lines are identical for each observed position. The error in the parentheses represents one standard deviation, which applies to the last significant digits.

Table 2. Observed line parameters toward the Pipe nebula along strip-2. ^a

	$\Delta\alpha$ (arcmin)	V_{LSR} (km s ⁻¹)	FWHM (km s ⁻¹)	T_{MB} (1612) (K)	T_{MB} (1665) (K)	T_{MB} (1667) (k)	T_{MB} (1720) (K)
Stem region	-16	3.26 (4)	1.45 (6)	-0.070 (4)	0.008 (3)	0.009 (4)	0.082 (4)
		3.84 (1)	0.54 (2)	-0.036 (7)	0.111 (5)	0.190 (6)	0.086 (8)
	-8	3.12 (2)	0.82 (4)	-0.078 (3)	0.039 (3)	0.038 (3)	0.088 (3)
		3.85 (1)	0.50 (2)	-0.063 (5)	0.041 (4)	0.134 (4)	0.089 (5)
	0	3.08 (3)	0.95 (6)	-0.084 (4)	0.044 (3)	0.054 (4)	0.118 (4)
		3.74 (1)	0.57 (2)	-0.083 (7)	0.022 (5)	0.138 (6)	0.082 (10)
	8	2.95 (1)	0.69 (2)	-0.092 (4)	0.076 (3)	0.028 (4)	0.129 (4)
		3.73 (1)	0.63 (2)	-0.114 (4)	0.023 (4)	0.160 (4)	0.132 (4)
	16	2.77 (1)	0.67 (3)	-0.096 (4)	0.047 (4)	-0.063 (5)	0.083 (4)
		3.55 (1)	0.89 (3)	-0.096 (4)	0.038 (3)	0.114 (4)	0.102 (3)
24	4.12 (2)	1.55 (5)	-0.041 (3)	-0.050 (3)	-0.100 (3)	0.021 (3)	
Bowl region	32	4.26 (1)	1.01 (2)	-0.056 (3)	-0.095 (3)	-0.162 (4)	0.015 (3)
	40	-	-	-	-	-	-
	48	4.27 (2)	1.33 (6)	-0.066 (3)	0.011 (3)	-0.084 (3)	0.063 (3)
		5.16 (1)	0.62 (3)	0.020 (5)	-0.072 (4)	-0.039 (6)	-0.036 (5)
	56	4.14 (2)	1.33 (4)	-0.069 (3)	0.032 (3)	-0.095 (4)	0.078 (3)
		5.25 (2)	1.38 (4)	0.020 (3)	-0.099 (3)	-0.137 (3)	-0.055 (3)
	64	4.22 (18)	1.69 (18)	-0.10 (2)	0.027 (6)	0.007 (7)	0.10 (2)
		4.95 (2)	1.31 (5)	0.03 (3)	-0.055 (9)	-0.144 (5)	-0.05 (3)
	72	3.79 (2)	1.23 (5)	-0.06 (1)	-0.003 (4)	0.03 (1)	0.058 (8)
		5.05 (4)	1.53 (17)	-0.09 (6)	-0.002 (13)	-0.12 (7)	0.07 (5)
	80	5.70 (60)	2.27 (41)	0.07 (4)	0.015 (8)	0.08 (5)	-0.06 (3)
		6.11 (2)	0.65 (4)	-0.009 (5)	-0.043 (5)	-0.094 (5)	-0.005 (4)

^a $\Delta\alpha$ in the first column denotes a R.A. offset from the $(\alpha_{2000}, \delta_{2000}) = (17^{\text{h}}27^{\text{m}}12^{\text{s}}.0, -26^{\circ}42'59.0'')$ position. The main beam temperatures (T_{MB}) of the four hfs line of OH, the V_{LSR} value, and the linewidth (FWHM) are obtained by a Gaussian fit, assuming that the V_{LSR} values and the linewidths of the four hfs lines are identical for each observed position. The error in the parentheses represents one standard deviation, which applies to the last significant digits.

Table 3. Observed line parameters toward the Pipe nebula along strip-3. ^a

$\Delta\delta$ (arcmin)	V_{LSR} (km s ⁻¹)	FWHM (km s ⁻¹)	T_{MB} (1612) (K)	T_{MB} (1665) (K)	T_{MB} (1667) (k)	T_{MB} (1720) (K)
8	4.16 (2)	1.20 (5)	-0.033 (3)	-0.065 (3)	-0.097 (4)	0.002 (3)
	5.84 (4)	1.2 (1)	-0.025 (3)	-0.042 (4)	-0.004 (3)	0.026 (3)
0	4.26 (1)	1.01 (2)	-0.056 (3)	-0.095 (3)	-0.162 (4)	0.015 (3)
-8	3.05 (1)	0.79 (2)	-0.160 (4)	-0.031 (4)	-0.155 (4)	0.103 (4)
	4.24 (1)	0.75 (2)	-0.080 (4)	-0.112 (4)	-0.210 (5)	0.047 (4)
-16	3.21 (2)	1.11 (5)	-0.102 (4)	-0.028 (3)	-0.094 (4)	0.049 (3)
	4.32 (1)	0.68 (2)	-0.065 (5)	-0.090 (4)	-0.198 (5)	0.021 (4)

^a $\Delta\delta$ in the first column denotes a Decl. offset from the the (32', 0') position on strip-2 (Table 2). The main beam temperatures (T_{MB}) of the four hfs line of OH, the V_{LSR} value, and the linewidth (FWHM) are obtained by a Gaussian fit, assuming that the V_{LSR} values and the linewidths of the four hfs lines are identical for each observed position. The error in the parentheses represents one standard deviation, which applies to the last significant digits.

Table 4. The derived parameters along strip-1.^a

$\Delta\delta$ (arcmin)	T_k (K)	$N(\text{OH})$ (10^{14} cm^{-2})	$T_{\text{cont}}(1667)$ (K)
16	58.6 (2)	1.13 (2)	4.5
8	48.3 (3)	1.00 (1)	4.6
0	42.9 (1)	1.178 (8)	4.7
-8	50.8 (2)	1.02 (1)	4.8
-16	58.8 (1)	1.27 (2)	4.9

^a $\Delta\delta$ in the first column denotes a Decl. offset from the $(\alpha_{2000}, \delta_{2000}) = (17^{\text{h}}20^{\text{m}}49^{\text{s}}.0, -26^{\circ}53'8.0'')$ position. The gas kinetic temperature (T_k) and the OH column density ($N(\text{OH})$) are determined from our statistical equilibrium calculation assuming the density and the ortho-to-para ratio of H_2 of 10^3 cm^{-3} and 3, respectively. The numbers in the parentheses represent one standard deviation of the fit in units of the last significant digits. T_{cont} in the last column is the intensity of the radio continuum background emission at the frequency of 1667 MHz evaluated from the HIPASS 1.4 GHz data (Calabretta et al. 2014).

Table 5. The derived parameters along strip-2.^a

	$\Delta\alpha$ (arcmin)	V_{LSR} (km s ⁻¹)	T_k (K)	$N(\text{OH})$ (10 ¹⁴ cm ⁻²)	$T_{\text{cont}}(1667)$ (K)
Stem region	-16	3.26	57.1 (2)	1.47 (3)	5.2
		3.84	45.6 (6)	0.63 (2)	5.2
	-8	3.13	55.0 (1)	0.93 (1)	5.2
		3.85	50.3 (3)	0.54 (1)	5.2
	0	3.08	54.2 (2)	1.19 (2)	5.3
		3.74	49.8 (5)	0.56 (3)	5.3
	8	2.95	54.2 (1)	0.95 (1)	5.3
		3.73	50.8 (2)	0.88 (1)	5.3
	16	2.77	57.6 (2)	0.79 (1)	5.4
		3.55	51.5 (2)	1.11 (2)	5.4
	24	4.12	66.6 (5)	0.85 (3)	5.5
Bowl region	32	4.26	73.6 (8)	0.53 (2)	5.5
	40	-	-	-	5.6
	48	4.27	59.2 (2)	1.25 (2)	5.6
		5.16	-	-	5.6
	56	4.14	58.1 (2)	1.35 (2)	5.7
		5.25	-	-	5.7
	64	4.22	54.3 (3)	1.9 (1)	5.7
		4.95	-	-	5.7
	72	3.79	55.9 (5)	0.93 (7)	5.7
		5.05	58 (1)	1.6 (3)	5.7
		5.70	-	-	5.7
	80	6.11	-	-	5.8

^a $\Delta\alpha$ in the first column denotes a R.A. offset from the $(\alpha_{2000}, \delta_{2000}) = (17^{\text{h}}27^{\text{m}}12^{\text{s}}.0, -26^{\circ}42'59.0'')$ position. The gas kinetic temperature (T_k) and the OH column density ($N(\text{OH})$) are determined from our statistical equilibrium calculation assuming the density and the ortho-to-para ratio of H₂ of 10³ cm⁻³ and 3, respectively. The numbers in the parentheses represent one standard deviation of the fit in the units of the last significant digits. T_{cont} in the last column is the intensity of the radio continuum background emission at the frequency of 1667 MHz evaluated from the HIPASS 1.4 GHz data (Calabretta et al. 2014).

Table 6. The derived parameters along strip-3.^a

$\Delta\delta$	V_{LSR} (km s ⁻¹)	T_k (K)	$N(\text{OH})$ (10 ¹⁴ cm ⁻²)	$T_{\text{cont}}(1667)$ (K)
8	4.16	73 (5)	0.43 (4)	5.5
	5.84	59 (1)	0.55 (4)	5.5
0	4.26	74 (2)	0.53 (2)	5.5
-8	3.05	62 (1)	1.00 (1)	5.6
	4.24	71 (2)	0.55 (2)	5.6
-16	3.21	61 (1)	1.03 (2)	5.6
	4.32	73 (2)	0.41 (2)	5.6

^a $\Delta\delta$ in the first column denotes a Decl. offset from the the (32', 0') position on strip-2 (Table 2). The gas kinetic temperature (T_k) and the OH column density ($N(\text{OH})$) are determined from our statistical equilibrium calculation assuming the density and the ortho-to-para ratio of H₂ of 10³ cm⁻³ and 3, respectively. The numbers in the parentheses represent one standard deviation of the fit in the units of the last significant digits. T_{cont} in the last column is the intensity of the radio continuum background emission at the frequency of 1667 MHz evaluated from the HIPASS 1.4 GHz data (Calabretta et al. 2014).